Journal of the Physical Society of Japan
Vol. 63, No. 12, December, 1994, pp. 4463–4474

Fermi Surface of Th within Local-Density Functional Theory

Masahiko HIGUCHI, Hiroshi YAMAGAMI[1] and Akira HASEGAWA[2]

Graduate School of Science and Technology, Niigata University, Niigata 950-21
[1]Department of Physics, Faculty of Science, Tohoku University, Sendai 980
[2]Department of Physics, Faculty of Science, Niigata University, Niigata 950-21

(Received June 15, 1994)

The energy band structure, particularly the Fermi surface, is calculated for fcc Th by a self-consistent, relativistic augmented-plane-wave method with the exchange and correlation potential in a local-density approximation. The extremal cross-sectional area of the Fermi surface is calculated carefully as a function of the direction of the normal on the {100} and {110} planes, which has been so far calculated only in three high-symmetry directions, and compared with the experimental results for the de Haas-van Alphen (dHvA) effect measured by Boyle and Gold (1969). As a result, it becomes possible to identify the origin of many dHvA frequency branches much more clearly. In addition, a new assignment of the theoretical and the experimental dHvA frequency branches is proposed, and the existence of several new dHvA frequency branches is predicted also.

[Th, band theory, local-density approximation, relativistic APW method, energy band structure, Fermi surface, density of states]

§1. Introduction

Th metal has attracted much interest and its electronic structure, particularly the Fermi surface, has been investigated both theoretically and experimentally, because it is located at the beginning of the actinide series, and its crystal structure is simple, i.e., it has the face-centered-cubic crystal structure below 1400°C. In Th, the $5f$ bands lie slightly above the Fermi level and affect the electronic structure in the vicinity of the Fermi level appreciably. Thus a careful investigation of the Fermi surface of Th is important as a first step toward a deep understanding of the nature of the $5f$ electrons in the actinides. In this paper, we investigate the electronic structure and the Fermi surface for Th in detail by band theory.

Its magnetic susceptibility increases slightly with temperature, and the room-temperature magnetic susceptibility is 9.7×10^7 emu/mole.[1] The low-temperature specific heat constant γ is reported to be 4.31 and 4.08 mJ/K^2 mole.[2] It was the first element in the actinide series for which the de Haas-van Alphen (dHvA) effect was measured, and the topology of the Fermi surface was suggested.[3,4] Soon later, the band calculations were performed in various methods to explain the Fermi surface shape and the cyclotron effective mass.

Gupta and Loucks[5] have first derived the Fermi surface for Th by a non-self-consistent calculation with a relativistic, augmented plane wave (APW) method. In their calculation, the Slater exchange potential was used, and the whole $5f$ bands appeared in the middle of the valence band. This result is unphysical, because the $5f$ bands should be almost unoccupied in Th. Therefore, Gupta and Loucks[5] removed them out artificially. The Fermi surface that they predicted is simple. It consists of a hole sheet centered at the Γ point ("rounded cube"), four hole sheets centered at the L points ("dumbbells") and twelve electron sheets which lie across the Σ axes ("lungs"). These three kinds of sheets explained the behavior of the experimental dHvA frequency branches qualitatively well. It was not easy, however, to identify the origin of the experimental dHvA frequency branches clearly, because they did not calculate the dependence of the dHvA frequencies on the direction of a magnetic field, but merely suggested it.[4] Furthermore, the quantitative disagreements be-

tween theory and experiment remained about the volume surrounded by hole sheets.

In order to clarify the influence of the $5f$ states on the Fermi surface, Koelling and Freeman[6] have investigated a change of the band structure by using the local exchange potential with a scale factor which varies from 1 to 2/3. The local exchange potential is derived with a crystal charge density which is generated by overlapping atomic charge densities obtained under an assumed configuration. Koelling and Freeman[6] suggested that both the decreasing in the exchange scale factor and the inclusion of the $5f$ states in the band structure could be in the correct direction to remove the disagreement between theory and experiment about the volume of hole sheets.

On the basis of an itinerant $5f$ electron model, Skriver and Jan[7] have performed the first self-consistent calculation for Th with a relativistic linear-muffin-tin-orbital (LMTO) method in the atomic-sphere approximation by using the exchange and correlation potential which is devised in the local-density approximation (LDA) by von Barth and Hedin.[8] By a self-consistent treatment, they confirmed the importance of the hybridization of the valence band with the $5f$ states stressed by Koelling and Freeman.[6] In order to fit the Fermi surface to the experimental results for the dHvA effect in the high-symmetry directions, they found it necessary to shift the Fermi level by 2 mRyd. for the cube, -14 mRyd. for the dumbbell, and -6 mRyd. for the lung. In all the previous calculations for Th, the dHvA frequencies have been calculated only in the high-symmetry directions of a magnetic field, and their angular dependence has been calculated neither on the {100} plane nor on the {110} plane.

On the basis of the itinerant $5f$ electron model, we have recently calculated the electronic structure and derived the Fermi surface for two interesting U compounds, UC and UB_{12}, by using a self-consistent, relativistic APW method with the exchange and correlation potential in the LDA.[9,10] We could explain reasonably well the magnitude and the angular dependence of the major experimental dHvA frequency branches without introducing any adjustable parameters.

In the light of our experience of these U compounds, the magnitude of the Fermi energy shifts that Skiver and Jan[7] introduced for Th seems to be somewhat too large. At present, it is not clear whether these errors should be ascribed to the inadequacy of the LDA and/or the shape approximation to the potential. Furthermore, the possibility that they may imply limitations of the relativistic LMTO method when it is applied to the actinides cannot be ruled out.

Judging from these previous studies on Th, it seems necessary to re-examine the Fermi surface for Th as carefully as possible even within the framework of conventional band theory which is based on the LDA. Some errors may be inevitable because of the simplification adopted in the treatment of the exchange and correlation potential and the spatial shape of the crystal potential. We believe it rather important, however, to clarify the property of limitations inherent in such band theory. It is possible to clarify a part of the limitations at least by investigating the Fermi surface carefully.

In this paper, within the framework of the LDA, we recalculate the energy band structure and derive the Fermi surface for Th by a method different from Skiver and Jan,[7] i.e., by a self-consistent, relativistic APW method, and investigate the angular dependence of the extremal cross-sectional areas of all sheets of the Fermi surface as carefully as possible. As a result, we find that theoretical results can explain the angular dependence of the available experimental dHvA frequency branches reasonably well. In addition, we propose a new assignment of the theoretical and experimental frequency branches which may be more reasonable than the previously suggested one, and also predict the existence of several new dHvA frequency branches, which hopefully may serve as a useful guide for future experimental investigations.

Organization of this paper is as follows. Method of calculation used in this paper is described in §2. Theoretical results for the energy band structure and the Fermi surface are explained in §3. Theoretical results are compared with experimental ones in §4. Finally, results are discussed in §5.

§2. Method of Calculation

To calculate the energy band structure for Th metal, we here apply a self-consistent, relativistic, symmetrized APW method with the exchange and correlation potential in the LDA. This method has been completed from Loucks' relativistic APW method[11] with improvements by incorporating the symmetrization of the relativistic APW bases with double space groups and self-consistent calculations.[12] In parallel with this method, we use its linealized version (RLAPW),[13] which has been completed on the basis of a relativistic linear band theory proposed by Takeda.[14] The RLAPW method has an advantage to the determination of the electronic structure, since the matrix elements of the Hamiltonian and the overlap integral are independent of the eigenvalue which should be determined. We have confirmed that these two relativistic APW methods yield the eigenvalues at general k points which are identical within 1 mRyd. The functional form of the exchange and correlation potential is the parameterization by Gunnarsson and Lundqvist.[15]

The shape of the one-electron potential is determined in the muffin-tin approximation. The radius of the APW sphere is chosen to be the half of the nearest-neighbor Th-Th distance, i.e., $a/2\sqrt{2}$, where a is the lattice constant. The APW spheres occupy 74% of the whole space in a crystal. The lattice constant and other crystal constants used in this calculation are listed in Table I.

A starting crystal charge density for the self-consistent iteration procedure is constructed by a superposition of the relativistic charge density for neutral Th atom (Rn, $6d^2 7s^2 5f^0$), which is calculated self-consistently with the relativistic method of Liberman *et al.*,[17] where Rn means the atomic configuration of Rn atom. In the atomic calculation, the same exchange and correlation potential form is used as in the crystal, and the spin-orbit splitting in the $6p$, $6d$ and $5f$ state is found to be 585 mRyd., 37 mRyd. and 48 mRyd., respectively. During the iterations, the Rn core states except the $6p^6$ state are treated in the frozen-core approximation.

Throughout this band structure calculation, about 320 relativistic APW basis functions and the total angular momenta up to 15/2 are used to expand the Bloch function. These numbers of the expansion correspond to 160 plane waves and the angular momenta up to 7, which are determined under the condition that the eigenvalues should converge well within a few mRyd.

Table I. Crystal constants of Th used in the calculation. The lattice constant is taken from ref. 16.

Crystal structure	FCC
Space group	Fm3m
Lattice constant, a	9.608316 a.u.
APW sphere radius	3.397053 a.u.

In each cycle of the self-consistent iteration processes, the charge density is calculated at nineteen k points, i.e., five symmetry points, seven points on the symmetry axes and seven points on the symmetry planes, which correspond to 256 points distributed uniformly over the full Brillouin zone. Using the final self-consistent charge density, the eigenvalues are calculated at many symmetry and general points, totally 231 points in the irreducible 1/48 parts of the Brillouin zone.

To obtain the density of states and the Fermi surface, the eigenvalues thus calculated are converted into energies at finer meshes with an interpolation by the Fourier series expansion. The density of states is calculated by the tetrahedron method.[18,19] The Fermi surface is represented in perspective by the aid of the computer program "TPERSP" made by A. Yanase at the Tohoku University Computer Center.

§3. Results of Calculation

3.1 Fully relativistic energy band structure

Figure 1 shows the result of this calculation for the energy band structure for Th along the symmetry axes in the Brillouin zone. The Fermi energy E_F is located at 0.6200 Ryd. Three $6p$ bands which lie in the energy region between -1.2 Ryd. and -0.4 Ryd. are omitted from Fig. 1. In the energy range below E_F, this result is similar to that of Gupta and Loucks[5] who used the Slater exchange and artificially removed the $5f$ bands. In addition, this result looks similar to the result of

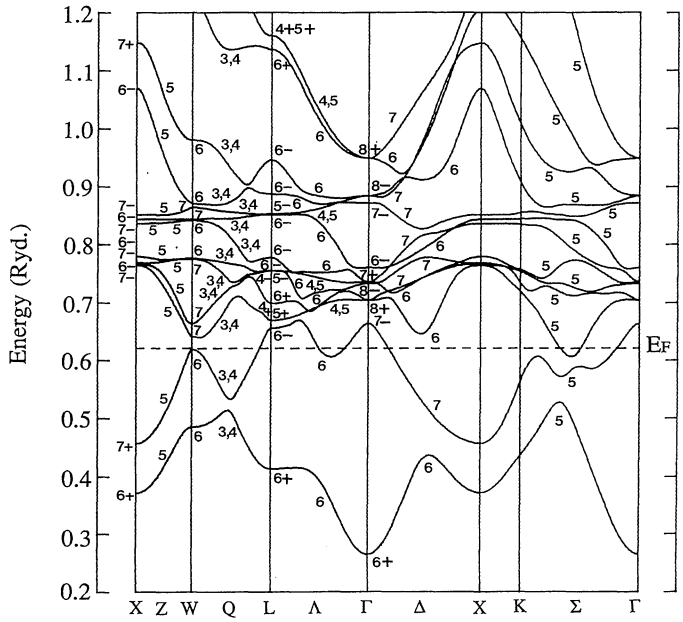

Fig. 1. Relativistic energy band structure for Th in the vicinity of the Fermi energy E_F.

Koelling and Freeman[6] with the exchange scale factor of 2/3 and also the result of Skriver and Jan[7] who used the exchange and correlation potential of von Barth and Hedin.[8]

In order to investigate the character of each band, the charge distributions for many states at the Γ point are partitioned according to the angular momenta, and listed in Table II. As is shown in Table II, at the Γ point, the lowest Γ_6^+ state consists dominantly of the s state.

Table II. Charge distributions partitioned into the angular momenta for the Bloch states at the Γ point. Components are shown in percent.

Band	Bloch state	Energy (Ryd.)	Outer region	Th APW sphere			
				s	p	d	f
1	Γ_6^+	0.264	35	64	0	0	0
2	Γ_7^-	0.663	11	0	0	0	88
3, 4	Γ_8^+	0.704	10	0	0	86	0
5	Γ_7^+	0.733	11	0	0	85	0
6, 7	Γ_8^-	0.735	6	0	0	0	93
8	Γ_6^-	0.760	7	0	0	0	92
9	Γ_7^-	0.871	0	0	0	0	99
10, 11	Γ_8^-	0.884	0	0	0	0	99
12, 13	Γ_8^+	0.948	5	0	0	91	0

The Γ_6^-, two Γ_7^- and two Γ_8^- that lie above it specify the f bands, while the Γ_7^+ and two Γ_8^+ states specify the d bands. Figure 1 shows that these states, especially the d states, form wide bands. The f bands split into two subbands which correspond to the total angular momenta $j=5/2$ (lower bands) and $7/2$ (upper bands), and the magnitude of the splitting is slightly greater than the spin-orbit splitting in the atomic $5f$ state because of the crystal field effect. As is shown in Fig. 1, the main part of the f bands exist just above E_F.

Although the d bands and the f bands do not hybridize at the Γ point, they do at other points with low symmetry. For example, along the Δ axis, the Δ_7 branch starts from the Γ_7^- state (0.663 Ryd.) with large dispersion. In this Δ_7 branch, the d states and the f states hybridize. At the X point, this branch is compatible with the X_7^+ state, in which the f components vanish and the d components become dominant. The Fermi surface is constructed by the second and the third bands, both of which contain the f components appreciably through the d-f hybridization. Thus, the $5f$ states may affect the Fermi surface, though the main part of the f bands are unoccupied, as

was first suggested by Koelling and Freeman.[6]

The number of the valence electrons in the APW sphere partitioned according to the angular momenta is 0.47(s), 6.00(p), 1.96(d) and 0.41(f). There are 1.22 valence electrons outside the APW sphere in the primitive cell. The value of the f component is a little smaller than that of Skriver and Jan,[7] who reported the value of 0.5 for the f state. The density of states is calculated at E_F as 16.2 states/Ryd. cell. The contribution from the f states to the density of states at E_F amounts to 30% of the total.

3.2 *The Fermi surface*

Figure 1 shows that the second and the third bands construct the Fermi surface. The second band constructs the hole sheets which consist of a rounded *cube* centered at the Γ point and four *dumbbells* centered at the L points, as is shown in Fig. 2. The dumbbell is stretched along the $\langle 110 \rangle$ direction and has *triangular ends* which are connected by the *hyperbolic neck*. The third band constructs the electron sheets which consist of twelve *lungs* which lie across the Σ axis, as is shown in Fig. 3. The lung consists of two *lobes* and a slender *junction*.

All these Fermi surface sheets are tiny and closed, so that they cannot hold open orbits.

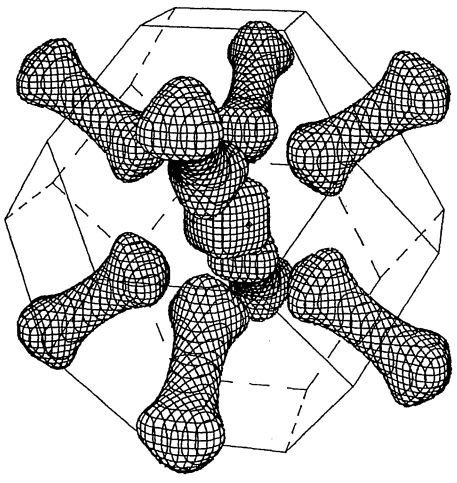

Fig. 2. The hole sheet of the Fermi surface in the second band for Th. The hole sheet consists of the rounded cube centered at the Γ point and the dumbbells centered at the L points.

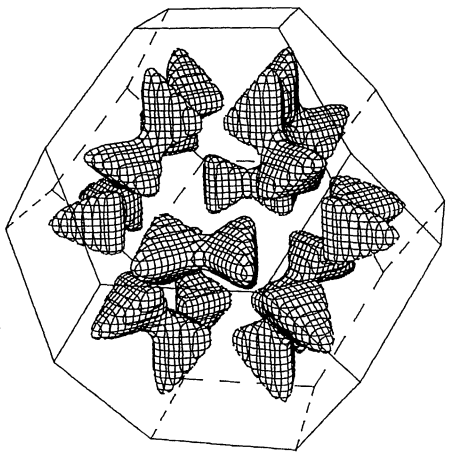

Fig. 3. The electron sheet of the Fermi surface in the third band for Th. The electron sheet consists of the lungs which lie across the Σ axes.

The hole sheets contain totally 0.14 holes/cell, and the electron sheets contain totally the same number of electrons. This result is consistent with the fact that Th metal has even number of electrons per primitive cell, i.e., it is a compensated metal.

3.3 *Extremal cross-sections of the Fermi surface*

We calculate the extremal cross-sectional area of the hole sheets and the electron sheets of the Fermi surface in various directions. The extremal cross-sectional area A is related to the dHvA frequency F by the well-known formula $F=(ch/2\pi e)A$. It can be written as $F[\mathrm{Oe}]=1.59936\times 10^8 A$ for Th, where A is measured in units of $(2\pi/a)^2$.

We use the same notations as those of the Gupta-Loucks model for the orbits except that the orbits ***c*** and ***d*** are interchanged in order to be consistent with Skriver and Jan,[7] and Koelling and Freeman.[6] In the present work, we have discovered many new orbits on the lung and the dumbbell. New orbits are the orbits ***r***, ***s*** and ***w*** on the lung and the orbits ***t***, ***v***, ***x*** and ***q*** on the dumbbell, and added in the following analysis.

Figure 4 shows the theoretical dHvA frequencies as functions of the magnetic-field direction on the {100} and {110} planes. In Fig. 4, the chain curve, dashed curves and

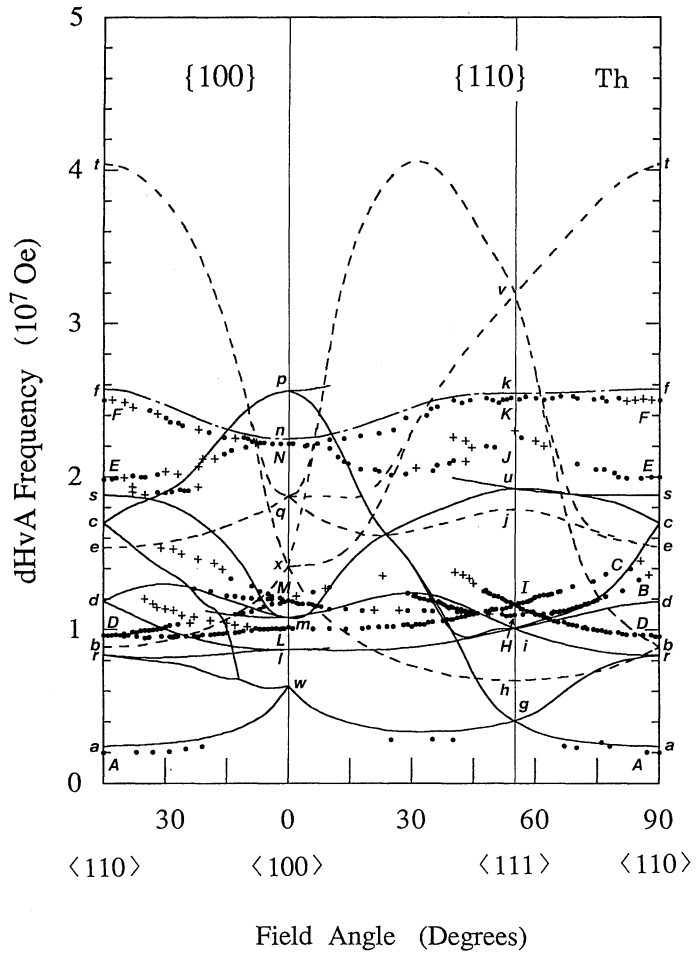

Fig. 4. Theoretical and experimental frequencies of the de Haas-van Alphen effect for Th as a function of the direction of a magnetic field on the {100} and {110} planes. The chain curve, the dashed curves and the solid curves show the frequencies calculated from the cube, the dumbbells and the lungs, respectively. Small circles and crosses show the experimental results of ref. 4. The alphabets and the Greek letters show the theoretical and experimental results, respectively.

solid curves show the dHvA frequency branches which are calculated from the cube, the dumbbells and the lungs, respectively. In the following, we explain from what orbit these theoretical branches originate on individual sheets of the Fermi surface.

3.3.1 Cube

The cube produces a single dHvA frequency branch which exists in all directions. Figure 5 shows three orbits n, f and k which run around it on the plane perpendicular to the 〈100〉, 〈110〉 and 〈110〉 directions, respectively.

3.3.2 Dumbbell

It is sufficient to deal with the orbits running on the four independent dumbbells, as is shown in the Fig. 6. In the 〈100〉 direction, there exist two kinds of orbits. One is x which runs around the L point with the minimum area, and another is q which runs around the triangular end with the maximum area. Since the orbits which run around the equivalent points on four independent dumbbells have the same areas in the 〈100〉 direction, both x and q are degenerate fourfold.

On the {100} and {110} planes, however,

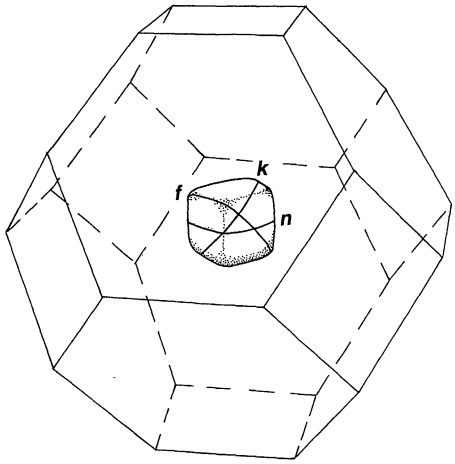

Fig. 5. Various extremal orbits on the cube, which are normal to the three high-symmetry directions: the orbits ***n***, ***f*** and ***k*** are normal to the ⟨100⟩, ⟨110⟩ and ⟨111⟩ directions, respectively.

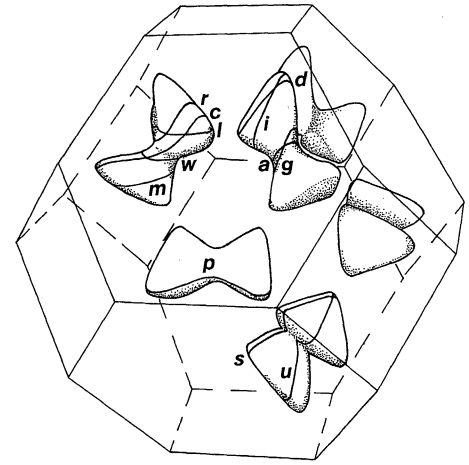

Fig. 7. Various extremal orbits on the lungs, which are normal to the three high-symmetry directions: the orbits ***l***, ***m***, ***p*** and ***w*** are normal to the ⟨100⟩ direction, the orbits ***a***, ***c***, ***d***, ***r*** and ***s*** to the ⟨110⟩ direction, and the orbits ***g***, ***i*** and ***u*** to the ⟨111⟩ direction.

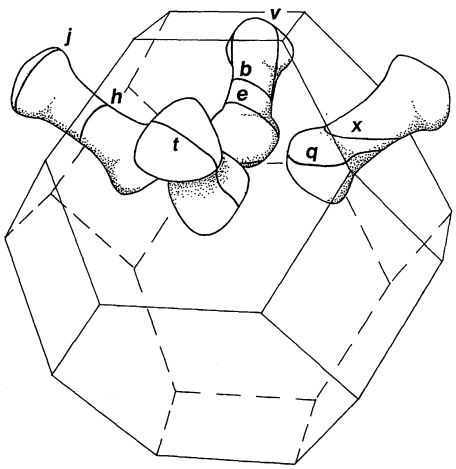

Fig. 6. Various extremal orbits on the dumbbells, which are normal to the three high-symmetry directions: the orbits ***q*** and ***x*** are normal to the ⟨100⟩ direction, the orbits ***b***, ***e*** and ***t*** to the ⟨110⟩ direction, and the orbits ***h***, ***j*** and ***v*** to the ⟨111⟩ direction.

the degeneracy is resolved. The orbit ***x*** splits into two branches on the {100} plane, which turn into the orbits ***b*** and ***t*** in the ⟨110⟩ direction. Both of them have the center near the hyperbolic neck. The orbit ***q*** also splits into two branches on the {100} plane. One of the two branches, which is denoted as ***e*** in the ⟨110⟩ direction, originates from the orbit running around the triangular end, while the other, which is denoted as ***t*** in ⟨110⟩ direction, has the center that moves near to the hyperbolic neck as the field angle goes toward the ⟨110⟩ direction.

On the {110} plane, the orbit ***x*** splits into three branches, all of which originate from the orbits running around the hyperbolic neck. These orbits are denoted as ***h*** and ***v*** in the ⟨110⟩ direction, and ***b*** and ***t*** in the ⟨110⟩ direction.

The orbit ***q*** also splits into three branches on the {110} plane. One of the three branches originates from the orbit running around the triangular end, and is denoted as ***j*** in the ⟨110⟩ direction and ***e*** in the ⟨110⟩ direction. Other two branches originate from the orbit, the center of which moves from the triangular end to the hyperbolic neck as the field angle varies from ⟨100⟩ to ⟨110⟩ on the {110} plane. Therefore, these branches are united with the branches which are separated from the orbit ***x***.

3.3.3 Lung

It is sufficient to seek the orbits that result from the six independent lungs, as is shown in Fig. 7.

In the ⟨100⟩ direction, there exist four kinds of orbits, i.e., ***w***, ***l***, ***m*** and ***p***. The orbit ***w*** originates from the orbit running around the junction part with the minimum area. The orbits ***l*** and ***m*** originate from the orbits running

on the lobe with the maximum area. The orbit p originates from the orbit with the largest cross-sectional area of the lung. It is easy to see that the orbit p is degenerate twofold, and the orbits m, l and w are degenerate fourfold in the ⟨100⟩ direction.

On the {100} and {110} planes, these degeneracies are resolved partly. The orbit w splits into three branches on the {100} plane, which are denoted as a, r and c in the ⟨110⟩ direction. The orbits r and c have the minimum and maximum areas, respectively. Their centers are kept apart, until they coincide with each other in the vicinity of 10° on the {100} plane.

The orbit l splits into two branches on the {100} plane, which are denoted as r and d in the ⟨110⟩ direction. Both branches originate from the orbits running around the lobe.

The orbit m also splits into three branches on the {100} plane. One of the three branches has the twofold degeneracy and disappears in the vicinity of 20°. Other two branches are denoted as d and s in the ⟨110⟩ direction.

On the {110} plane, all branches which are separated from the orbits w, l and m are degenerate twofold. There exists only one branch from the orbit w on the {110} plane, which is denoted as g in the ⟨110⟩ direction and r in the ⟨110⟩ direction. As the field angle increases on the {110} plane, its center shifts in the direction from the junction part toward the lobe.

The orbit l splits into two branches on the {110} plane. One of the two branches becomes the orbit i in the ⟨110⟩ direction and the orbit c in the ⟨110⟩ direction. Another branch disappears in the vicinity of 10°.

The orbit m also splits into two branches on the {110} plane. These two branches have the extremal orbits i and u in the ⟨110⟩ direction, and r and c in the ⟨110⟩ direction.

The orbit p splits into two branches on the {110} plane. One of the two branches turns into the orbit u in the ⟨110⟩ direction and the orbit s in the ⟨110⟩ direction. It disappears in the angle range between 10° and 40° on the {110} plane. Another branch splits into two branches nearby 40°. The branch with a larger frequency originates from the maximum orbit on a lung, and coincides with the orbit i in the ⟨110⟩ direction and the orbit d in the ⟨110⟩ direction. The branch with a smaller frequency originates from the minimum orbit, and coincides with the orbit g in the ⟨110⟩ direction and the orbit a in the ⟨110⟩ direction.

§4. Comparison with Experiments

In this section, we compare the theoretical results for the dHvA frequencies, the cyclotron effective masses and the density of states with experimental results.

4.1 dHvA frequency branches

In Fig. 4, we show the theoretical dHvA frequency branches together with the experimental results of Boyle and Gold.[4] The experimental and theoretical orbits which are thought to have the same origin are labeled with the same capital and small letter, respectively, except for the experimental orbit D.

(A) Cube

(1) The theoretical branch ***n-k-f*** may correspond to the experimental branch ***N-K-F*** because of similar angular dependence and magnitude in the whole range of angles.

(B) Dumbbell

The frequency branches that are calculated from the dumbbell can explain the behavior of some experimental branches, though the quantitative agreement between theory and experiment is not so good as for the cube. In the ⟨100⟩ direction, the theoretical orbit q is not observed in the experiment. Therefore, the corresponding hypothetical orbit in this direction is supposed to be Q' for the sake of the following explanations. The magnitude of Q' may be slightly larger than that of the orbit N.

(2) On the {100} plane, the experimental branch ***E-Q′*** may be assigned to the theoretical branch ***e-q*** because of the similar angular dependence.

(3) On the {110} plane, the experimental branch ***Q′-J-E*** may be assigned to the theoretical branch ***q-j-e*** because of the similar angle dependence.

(4) On the {110} plane, the experimental branch ***H-B*** may correspond to a part of the theoretical branch ***x-h-b***.

(C) Lung

The branches which originate from the lung

can explain many experimental branches fairly well.

(5) The previous assignment (*d*, *D*)[4-7] seems unreasonable to us, because on the {110} plane the angle dependence of the branch ***I-D*** contradicts that of the branch ***i-d***. We suggest that the assignment (*r*, *D*) may be reasonable, because on the {110} plane the angle dependence of the branch ***I-D*** resembles that of the branch ***i-r***.

The theoretical orbit ***d*** may be missed in the experiment. Therefore, the corresponding hypothetical orbit is supposed to be ***D′*** for the sake of the following discussions. The orbit ***D′*** should be observed in the range between ***C*** and ***D*** in the ⟨110⟩ direction.

(6) On the {110} plane, the experimental branch ***L-I-C*** may be assigned to the theoretical branch ***l-i-c***.

(7) On the {110} plane, the experimental branch ***M-I-D*** may be assigned to the theoretical branch ***m-i-r***.

(8) On the {100} plane, the experimental branch ***L-D*** may be assigned to the theoretical branch ***l-r***.

(9) A part of the theoretical branch ***m-u-c*** may be observed in the angle range from 0° to 10° on the {110} plane.

(10) The theoretical branch ***p-i-d*** seems to be partly observed in the narrow angle range from 40° to 55°. The unobserved branch ***I-D′*** may follow it.

(11) On the {100} plane, the theoretical branch ***l-d*** may correspond to the experimental branch ***L-D′***, though the latter branch is not observed in the vicinity of the ⟨110⟩ direction.

(12) On the {100} plane, the three experimental branches that are separated from the orbit ***M*** may be assigned to a part of the theoretical branch ***m-s***, a part of the theoretical branch ***m-d***, and the theoretical branch that disappears nearby 20°, respectively.

(13) On the {100} plane, the theoretical branch ***w-a*** is partly observed in the angle range from 20° to 45°. On the {110} plane, the theoretical branch ***g-a*** is partly observed in the angle range from 65° to 90°, and the branch ***w-g*** around 30°.

(14) On the {100} plane, the theoretical branch ***p-c*** seems to be partly observed in the vicinity of 30°.

There are theoretical branches which have not been confirmed in the experiment, as is shown in Fig. 4. An origin of the experimental branch which starts from ***D*** in the ⟨110⟩ direction and slightly increases on the {100} plane is not clear. The disagreements between theory and experiment will be discussed in the next section.

4.2 Cyclotron effective mass

The ratio of the cyclotron effective mass m_c^* to the free-electron mass m_0 can be expressed as $m_c^*/m_0 = 0.13612 \times dA/dE$ for Th. The ratio is calculated for each theoretical dHvA frequency in the three high-symmetry directions, and listed together with the previous theoretical results and the experimental results in Table III. Compared with the theoretical results by Skriver and Jan,[7] our results for m_c^* are a little larger on the average, and approach closer to the experimental results. However, decisive disagreements between theory and experiment remain, and should be ascribed to many-body effects which band theory fails to take into account. The enhancement factor for m_c^* due to such many-body effects may be defined as $\lambda_c = (m_c^*)_{exp}/(m_c^*)_{band} - 1$, though it may vary from orbit to orbit. From Table III, we obtain $\lambda_c = 0.21 \sim 0.74$ as far as the four experimental values for m_c^* are used.

4.3 Density of states

The density of states is calculated at E_F as 16.2 states/Ryd. cell, which corresponds to the electronic specific heat constant due to the band structure γ_{band} of 2.81 mJ/K^2 mole. The experimental value for γ is $\gamma_{exp} = 4.08$ mJ/K^2 mole and 4.31 mJ/K^2 mole,[2] which may be renormalized similar to m_c^*. Thus, the enhancement factor for γ is defined as $\lambda = \gamma_{exp}/\gamma_{band} - 1$. We obtain $\lambda = 0.45 \sim 0.53$. Quantitatively, this result does not contradict the magnitude of the enhancement factors found for m_c^*.

Figure 8 shows the theoretical density of states (DOS) for occupied and unoccupied bands as a function of energy, which is convoluted with the Gaussian with the half width of 20 mRyd., together with the experimental DOS observed by means of the X-ray photo-

Table III. Theoretical and experimental results of the extremal cross-sectional areas and the cyclotron effective masses in the three high-symmetry directions for Th. The cross-sectional area and the cyclotron effective mass are measured in units of $(2\pi/a)^2$ and the free-electron mass, respectively.

Sheet	Direction	Orbit	External areas						Effective masses			
			expt.[a]	expt.[b]	calc.[c]	calc.[d]	calc.[b]	calc.[f]	expt.[e]	calc.[c]	calc.[d]	calc.[f]
Cube	⟨100⟩	N	22.1	22.1	22.5	22.9	21.1	21.6	−0.75±0.03	−0.645	−0.62	−0.55
	⟨110⟩	F	25.1	24.7	25.7	26.6	23.5	24.2		−0.892	−0.88	−0.72
	⟨111⟩	K	25.1	25.2	25.4	26.3	23.7	24.3		−0.835	−0.85	−0.69
Dumbbell	⟨110⟩	B	13.5	13.5	8.9	9.8	12.0	12.4		−0.315	−0.25	−0.37
	⟨110⟩	E	20.0	19.8	15.4	15.6	18.3	18.7		−0.402	−0.34	−0.41
	⟨111⟩	H	10.9	10.9	6.7	7.9	9.3	9.6		−0.228	−0.19	−0.27
	⟨111⟩	J	22.4	22.4	17.9	16.7	21.4	21.8		−0.506	−0.41	−0.48
	⟨100⟩	Q			18.7	16.0		21.8		−0.519	−0.52	−0.81
Lung	⟨110⟩	A	2.5	2.014	2.4	1.7	1.74	1.6		0.217	0.15	0.20
	⟨110⟩	C	15.9	15.9	17.0	12.0	14.3	13.6		0.775	0.60	0.67
	⟨110⟩	D	9.6	9.6	8.36(r)	8.6	8.7	8.3	0.58±0.01	0.339(r)	0.32	0.44
	⟨100⟩	L	10.0	10.0	8.7	8.9	10.0	9.9	0.66±0.03	0.465	0.38	0.55
	⟨111⟩	G			4.1			30.3		0.374		0.43
	⟨111⟩	I	11.7		10.1			10.9		0.384		0.40
	⟨100⟩	M	11.8		10.7	10.6		11.2	0.58±0.03	0.373	0.35	0.34
	⟨100⟩	P			25.6	21.5		21.8		0.536	0.63	0.71

a Boyle and Gold[4] as quoted by Koelling and Freeman.[6]
b Schirber, Schmidt and Koelling.[21]
c Present work.
d Skriver and Jan.[7]
e Boyle and Gold.[4]
f Koelling and Freeman.[6]

emission spectroscopy (XPS) and the bremsstrahlung isochromat spectroscopy (BIS) by Baer and Lang.[20] The XPS and BIS results are adjusted to the same intensity at the Fermi energy. The theoretical result is normalized arbitrarily so that it has the same peak height above the Fermi energy as the experimental result.

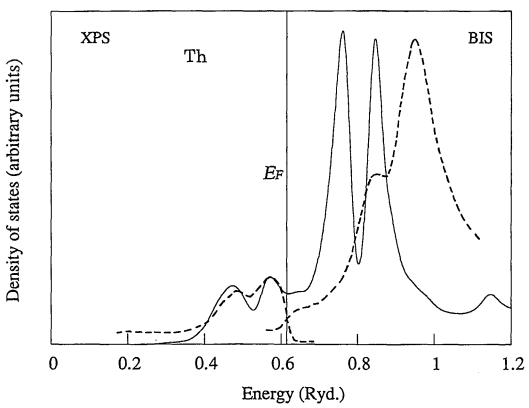

Fig. 8. The density of states as a function of energy for Th. The solid curve and the dashed curve show the theoretical density of states and the experimental XPS-BIS spectra of ref. 19, respectively. The theoretical density of states is convoluted with the Gaussian with the half width of 20 mRyd. The experimental XPS-BIS spectra are adjusted to the same intensity at the Fermi energy.

Below the Fermi level, the XPS spectrum has two humps, and this structure looks similar to the theoretical one. Therefore, the origin of these two humps may be ascribed to the van Hove singularities which exist along the Δ axes and the Σ axes in the d bands, as is seen in Fig. 1.

Above the Fermi level, the theoretical DOS has two peaks with about the same height originating from the f bands, which split into two subbands due to the spin-orbit interaction and the crystal field effect. The BIS spectrum has two peaks too, but their height is much different. Moreover, the peaks are shifted to high energy by about 0.1 Ryd., and their width is extremely broadened. These large disagreements are not surprising, however, be-

cause the density-functional theory should be applied essentially to the ground state, whereas the experiments involve excited states with high energies.

§5. Discussions

In Table III, the results of the calculation for the dHvA frequencies of all branches in the three high-symmetry directions are listed together with the previous theoretical results and the experimental results. Here we compare our results with the results by Skriver and Jan,[7] because their calculation is the only previous calculation that was carried out self-consistently.

For the cube, their results for the dHvA frequency are larger by 4%~8% in the three high-symmetry directions than the experimental results, while our results are larger by 1%~4% than the experimental ones. For the dumbbell, their results are smaller by 22%~28% than the experimental ones, while our results are smaller by 20%~34% than the experimental ones. For the lung, their results are smaller by 10%~32% than the experimental ones, while our results are smaller by 4%~14% (and larger by 7% for the orbit C) than the experimental ones. Thus, for the cube and the lung, our results are in better agreement with the experimental results than their results. For the dumbbell, however, band theory has not been improved much.

It is clear that the dumbbell and the lung are a little too small in size, and also the dumbbell is too slender in shape, in agreement with the conclusion of Skriver and Jan.[7] Their calculational method was different from ours, i.e., they used a relativistic LMTO method and the exchange and correlation potential by von Barth and Hedin,[8] while we here use a relativistic APW method and the exchange and correlation potential by Gunnarsson and Lundqvist.[15] We are led to conclude that the disagreements between theory and experiment should be ascribed neither to the relativistic LMTO method nor to the relativistic APW method, but rather to limitations of the LDA and/or the muffin-tin approximation to the spatial shape of the potential.

Although band theory still should be improved, in the present work it becomes possible by a careful investigation on the angular dependence of the dHvA frequencies to identify the origin of many experimental branches much more clearly than previously. Furthermore, we can suggest that the new assignment (r, D) may be more reasonable than the assignment (d, D) which was previously proposed,[4-7] and also predict the existence of several new dHvA frequency branches.

Unfortunately, there are some theoretical branches which have not been confirmed, partly or entirely, in the available experiment. The intensity of the dHvA signals for the orbit whose area changes abruptly with the wave vector component parallel to a magnetic field becomes weak. For instance, it may not be easy to observe the branch w-a in the vicinity of the ⟨100⟩ direction, unless a sample of high purity is used in a measurement.

As is seen in Fig. 4, on the {100} plane there is an experimental dHvA branch which starts from D in the ⟨110⟩ direction, slightly increases and disappears at about 25°. This experimental branch is expected to originate from the lung, but actually its origin can be found neither on the lung in our calculation nor on any lungs which have been proposed previously.[4-7] The reason for this disagreement between theory and experiment is not clear. In order to solve remaining problems on the Fermi surface of Th, an improvement of the measurement of the dHvA effect in Th is highly desirable. We hope that our theoretical results will serve as a useful guide for future studies.

References

1) J. D. Greiner and J. F. Smith: Phys. Rev. B4 (1971) 3275.
2) J. E. Gordon, H. Montgomery, R. J. Noer, G. R. Pichett and R. Torbon: Phys. Rev. **152** (1966) 432.
3) A. C. Thorsen, A. S. Joseph and L. E. Valby: Phys. Rev. **162** (1967) 574.
4) D. J. Boyle and A. V. Gold: Phys. Rev. Lett. **22** (1969) 461.
5) R. P. Gupta and T. L. Loucks: Phys. Rev. Lett. **22** (1969) 458; Phys. Rev. B3 (1971) 1834.
6) D. D. Koelling and A. J. Freeman: Phys. Rev. B12 (1975) 5622.
7) H. L. Skriver and J.-P. Jan: Phys. Rev. B21 (1980) 1489.
8) U. von Barth and L. Hedin: J. Phys. C5 (1972) 1629.
9) A. Hasegawa and H. Yamagami: J. Phys. Soc. Jpn.

59 (1990) 218.
10) H. Yamagami and A. Hasegawa: J. Phys. Soc. Jpn. **60** (1991) 987.
11) T. L. Loucks: *Augmented Plane Wave Method* (Benjamin, New York, 1967).
12) H. Yamagami and A. Hasegawa: J. Phys. Soc. Jpn. **59** (1990) 2426.
13) M. Higuchi and A. Hasegawa: in preparation.
14) T. Takeda: J. Phys. F **9** (1979) 815.
15) O. Gunnarsson and B. I. Lundqvist: Phys. Rev. B**13** (1976) 4274.
16) P. Villars and L. T. Calvert: *Pearson's Handbook of Crystallographic Data for Intermetallic Phases* (American Society for Metal, 1985) Vol. 3, p. 3234.
17) D. Liberman, J. T. Waber and D. T. Cromer: Phys. Rev. **137** (1965) A27.
18) O. Jepson and O. K. Anderson: Solid State Commun. **9** (1971) 1763.
19) J. Rath and A. J. Freeman: Phys. Rev. B**11** (1975) 2109.
20) Y. Baer and J. K. Lang: Phys. Rev. B**21** (1980) 2060.
21) J. E. Schirber, F. A. Schmidt and D. D. Koelling: Phys. Rev. B**16** (1977) 4235.